

Fabrication and characterization of MgB_2 spherical shells with reduced thickness on 1 mm diameter Si_3N_4 spheres

Ruining Sun(孙瑞宁), Tiequan Xu(徐铁权), Yue Wang(王越), Furen Wang(王福仁), Zizhao Gan(甘子钊)
Citation: Chin. Phys. B, 2025, 34 (**7**): 077402. DOI: 10.1088/1674-1056/adcdec
http://cpb.iphy.ac.cn; http://iopscience.iop.org/cpb

What follows is a list of articles you may be interested in

Half-integer Shapiro steps in MgB_2 focused He ion beam Josephson junctions

Dali Yin(殷大利), Xinwei Cai(蔡欣炜), Tiequan Xu(徐铁权), Ruining Sun(孙瑞宁), Ying Han(韩颖), Yan Zhang(张焱), Yue Wang(王越), and Zizhao Gan(甘子钊)
Chin. Phys. B, 2024, 33 (**8**): 087404. DOI: 10.1088/1674-1056/ad4d62

Effects of irradiation on superconducting properties of small-grained MgB_2 thin films

Li Liu(刘丽), Jung Min Lee, Yoonseok Han, Jaegu Song, Chorong Kim, Jaekwon Suk, Won Nam Kang, Jie Liu(刘杰), Soon-Gil Jung, and Tuson Park
Chin. Phys. B, 2023, 32 (**12**): 127402. DOI: 10.1088/1674-1056/acf5d3

First-principles study of moderate phonon-mediated pairing in high-pressure monoclinic phase of BiS_2-based superconductors

Jie Cheng(程杰), Yu-Lan Cheng(程玉兰), Bin Li(李斌), and Sheng-Li Liu(刘胜利)
Chin. Phys. B, 2023, 32 (**10**): 107401. DOI: 10.1088/1674-1056/accd56

Flux pinning evolution in multilayer Pb/Ge/Pb/Ge/Pb superconducting systems

Li-Xin Gao(高礼鑫), Xiao-Ke Zhang(张晓珂), An-Lei Zhang(张安蕾), Qi-Ling Xiao(肖祁陵), Fei Chen(陈飞), and Jun-Yi Ge(葛军饴)
Chin. Phys. B, 2023, 32 (**3**): 037402. DOI: 10.1088/1674-1056/ac89e1

Anisotropic superconducting properties of $FeSe_{0.5}Te_{0.5}$ single crystals

Jia-Ming Zhao(赵佳铭) and Zhi-He Wang(王智河)
Chin. Phys. B, 2022, 31 (**9**): 097402. DOI: 10.1088/1674-1056/ac5610

Fabrication and characterization of MgB_2 spherical shells with reduced thickness on 1 mm diameter Si_3N_4 spheres

Ruining Sun(孙瑞宁)[1], Tiequan Xu(徐铁权)[1,2], Yue Wang(王越)[1,†], Furen Wang(王福仁)[1], and Zizhao Gan(甘子钊)[1]

[1] *Applied Superconductivity Center, State Key Laboratory for Mesoscopic Physics, School of Physics, Peking University, Beijing* 100871, *China*
[2] *Beijing National Laboratory for Molecular Sciences, Huairou Research Center, Institute of Chemistry, Chinese Academy of Sciences, Beijing* 100190, *China*

(Received 8 February 2025; revised manuscript received 6 April 2025; accepted manuscript online 17 April 2025)

Magnetic levitation of the fusion target by coating a thin MgB_2 superconducting shell on its outer surface has recently been proposed in inertial confinement fusion (ICF) to realize a noncontact support of the target at ~ 20 K to boost the implosion performance and fusion yield. To avoid possible effects on target ablation, the coated MgB_2 shell is anticipated to be as thin as possible while fulfilling the target levitation requirements. Under this circumstance, the fabrication of an MgB_2 shell with reduced thickness has been explored using a hybrid physical-chemical vapour deposition method. By gradually decreasing the deposition time, a set of MgB_2 shells were grown on 1 mm diameter Si_3N_4 spheres with the thickness reducing from 720 nm to 200 nm. The spherical shells all have a polycrystalline structure characterized by closely packed hexagonal grains, with both the grain size and thickness diminishing as the shell thickness decreases. The superconducting transition temperature T_c of the shells, as determined by both resistance and magnetization measurements, is in the range of 38–40 K and all shells exhibit ideal diamagnetism at low temperatures. For the thinnest shell of 200 nm, the superconducting critical current density J_c at 20 K reaches 8.0×10^6 A/cm^2 and 2.1×10^5 A/cm^2 under zero and 2 T applied field, respectively. The results indicate that it is experimentally feasible to fabricate MgB_2 spherical shells with a thickness as low as 200 nm while maintaining the high T_c and J_c, thereby taking a further step towards the application of the shell in superconducting magnetic levitation for ICF.

Keywords: superconducting spherical shells, MgB_2, HPCVD, critical current density

PACS: 74.78.–w, 74.70.Ad, 81.15.Gh, 74.25.–q

DOI: 10.1088/1674-1056/adcdec **CSTR:** 32038.14.CPB.adcdec

1. Introduction

Superconducting spherical shells (hollow spheres) have found applications in important fields. They are core components of the superconducting gyroscopes and gravimeters.[1,2] Through sustained efforts in various aspects, including the perfection of shell fabrication, significant advancements have been achieved in the development and application of superconducting gyroscopes and gravimeters, as exemplified by the notable success of the Gravity Probe B (GP-B) experiment and the deployment of superconducting gravimeters.[3–6] Because the superconducting spherical shells used are made from low transition temperature (T_c) superconductors, mostly Nb ($T_c \sim 9.2$ K in bulk), the operating temperature of such devices is usually limited at or below 4.2 K.[1–6] In this regard, MgB_2, with a $T_c \sim 39$ K in bulk,[7] might be considered for use in these areas, with the hope of substantially increasing the operating temperature, thereby reducing the cryogenic costs and restrictions.

The use of MgB_2 to fabricate the superconducting spherical shell has recently attracted particular interest for potential application in another important field, namely, inertial confinement fusion (ICF).[8,9] In the last two years or so, the National Ignition Facility of USA has achieved the long-sought ignition in indirect-drive ICF multiple times, generating great excitement and bringing increased attention worldwide to nuclear fusion which promises near-limitless clean energy.[10,11] It has been pointed out that realizing a more spherical implosion by reducing imperfections in the target capsule (a hollow sphere filled with the hydrogen isotopes deuterium and tritium) is one of the keys to achieving the ignition.[10] Previous studies have shown that the thin membrane, conventionally used to hold the target capsule in place within the hohlraum and thus coming into contact with the capsule, is one of the most significant factors contributing to implosion degradation by introducing perturbations to its spherical symmetry.[9,12] As a result, a non-contact support scheme by magnetically levitating the capsule with a superconducting spherical shell coated on its outer surface has been proposed recently, which, unlike the contact support method, would preserve the spherical symmetry of the capsule, thereby helping to improve the implosion performance and fusion yield.[8,9] To implement such a scheme, it is noted that, due to the cryogenic temperature of the deuterium–tritium fuel being restricted to ~ 20 K,[13] the superconducting material used to fabricate the spherical shell must possess a considerably high T_c. Furthermore, this material should be composed of elements with a low atomic

†Corresponding author. E-mail: yue.wang@pku.edu.cn

© 2025 Chinese Physical Society and IOP Publishing Ltd. All rights, including for text and data mining, AI training, and similar technologies, are reserved.

number Z as dictated by the capsule ablation process.[14,15] Among the superconductors, MgB_2, showing a high enough T_c and made of relatively light elements, seems to best fulfill these requirements.[8,9] Consequently, experimental efforts have been devoted in recent years to investigating the fabrication of MgB_2 spherical shells to explore their prospects in ICF applications.[16–18] Using Mg vapour annealing or the solid-phase diffusion method, MgB_2 spherical shells have been successfully grown by Bayu Aji *et al.*[16] on 2 mm diameter diamond spheres, albeit with a degradation in T_c to approximately 33 K or 24 K, respectively. We have also performed the deposition of MgB_2 spherical shells with a thickness of 1–2 μm on 2 mm and 1 mm diameter Si_3N_4 spheres by using a hybrid physical-chemical vapour deposition (HPCVD) method.[17,18] Initially, the MgB_2 spherical shells showed a $T_c \sim 33$ K,[17] but through optimization of the deposition parameters, the T_c was restored to 38–40 K for both 2 mm and 1 mm diameter spherical shells, that is, close to the value in bulk MgB_2, thereby holding promise for the shell for ICF applications.[18]

To further advance the practical application of MgB_2 superconducting shells in ICF, it is noted that coating the MgB_2 shell on the outer surface (the ablator) of the target capsule may cause issues to the capsule ablation process, as the thickness as well as the composition of the ablator layers would be altered. Careful design and consideration of the ablator layers are known to be vital for the ablation process and implosion quality.[14,19–21] Therefore, to avoid or minimize any potential impact on the capsule ablation, it is desirable for the coated MgB_2 spherical shell to be as thin as possible while still fulfilling the task of capsule levitation. It was previously estimated that, by meeting these requirements, the thickness of the MgB_2 shell could be around 100–200 nm.[8,17] With these in mind, we have conducted an experimental exploration in the present work to fabricate MgB_2 spherical shells with thickness reduced to the sub-micron scale and investigate how the microstructure and superconductivity of these shells evolve as their thickness decreases. By tuning the growth parameters, a set of MgB_2 spherical shells has been fabricated with thickness varying from 720 nm to 200 nm. Importantly, all shells display a high T_c of 38 K to 40 K and ideal diamagnetism at low temperatures, much like our previous observations in thicker MgB_2 shells. For the 200 nm thick shell, a zero-field superconducting critical current density J_c of 8.0×10^6 A/cm^2 at 20 K is shown, comparable to that reported in high-quality epitaxial MgB_2 thin films. It demonstrates that MgB_2 spherical shells, while retaining excellent superconductivity, can be successfully fabricated with their thickness falling into the range acceptable for ICF, which brings us closer to a practical application of the shell in this important field.

2. Experimental details

The MgB_2 spherical shells were deposited on 1 mm diameter polycrystalline Si_3N_4 spheres using the HPCVD method.[22,23] Throughout the deposition, the chamber was maintained at a pressure of 4 kPa by filling purified H_2 gas in a flow rate of 300 sccm (standard cubic centimetres per minute). Pure Mg source with high Mg vapour pressure was generated near the Si_3N_4 sphere upon heating Mg ingots to melt at about 650–700 °C, which were arranged to encircle the sphere. The MgB_2 shell deposition was triggered by the supply of B_2H_6 gas (5% in H_2) into the chamber, whose thermal decomposition provided the pure B source to react with Mg vapour thereby forming MgB_2 on the sphere. The thickness of the MgB_2 shell is determined by both the flow rate and the supply time of the B_2H_6 gas. In our previous work, the flow rate of the B_2H_6 gas was optimized to be 4 sccm for the deposition of MgB_2 spherical shells,[17,18] and accordingly in the present work we kept it at this value and chose to adjust the supply time of the B_2H_6 gas, namely, the deposition time, to tune the shell thickness. During the deposition, the Si_3N_4 sphere was rotated to ensure uniform coating of the MgB_2 over the whole spherical surface, as described in detail previously.[18]

To measure the shell thickness, a cross section of the MgB_2 shell was prepared and then inspected by a scanning electron microscope (SEM, FEI NOVA Nano-SEM 430). Two methods were utilized to obtain the cross section of the MgB_2 shell. The first one was to cut the shell-coated sphere into two hemispheres by using a diamond wire saw (Kejing STX-202A), similar to previous works.[17,18] In the present work, another approach was also employed, that is, to partially remove the MgB_2 shell over the spherical surface using conventional photolithography and wet etching in a phosphoric acid solution. Results from the two methods, namely, the wire-cutting method and the wet-etching method, were found to be consistent with each other, as will be demonstrated in the next section. With the SEM, surface morphology of the MgB_2 shell was also imaged.

Both electrical transport and magnetization measurements were performed to explore the superconducting transition of the MgB_2 shell. Under the traditional four-probe configuration, the temperature dependence of the resistance was measured in a physical property measurement system (PPMS) by increasing the temperature (from 4 K to 300 K) at a sweep rate of 2 K/min.[18] The magnetization measurements were conducted in a magnetic property measurement system (MPMS) operating in the vibrating sample magnetometer (VSM) mode. The magnetic moment (m) as a function of temperature was recorded under an applied field (H) of 20 Oe after zero field cooling (ZFC). To evaluate the superconducting critical current density J_c of the shell, m–H hysteresis

loops at fixed temperatures were measured in a field range of ±40 kOe at a sweep rate of 100 Oe/s.

3. Results and discussion

To fabricate MgB_2 spherical shells with reduced thickness, we shortened the deposition time. By decreasing it gradually from 32 min to 12 min, a set of MgB_2 shells has been obtained. To check the shell thickness, cross sections of the shells have been prepared and imaged. The cross sections were prepared from the wire-cutting method[17,18] or the wet-etching method, as described earlier. Figure 1 shows typical SEM images of the cross sections produced from the wet-etching method, with the deposition time varying from 32 min (Fig. 1(a)), 20 min (Fig. 1(b)), 14 min (Fig. 1(c)), to 12 min (Fig. 1(d)). The images show that the cross sections are easy to distinguish because the contrast between the MgB_2 shells and the underlying Si_3N_4 spheres is clear, and this makes them suitable for determining the thicknesses of the shells. We can see from Fig. 1 that as the deposition time was shortened, the thickness of the shell was reduced, in line with the initial expectations.

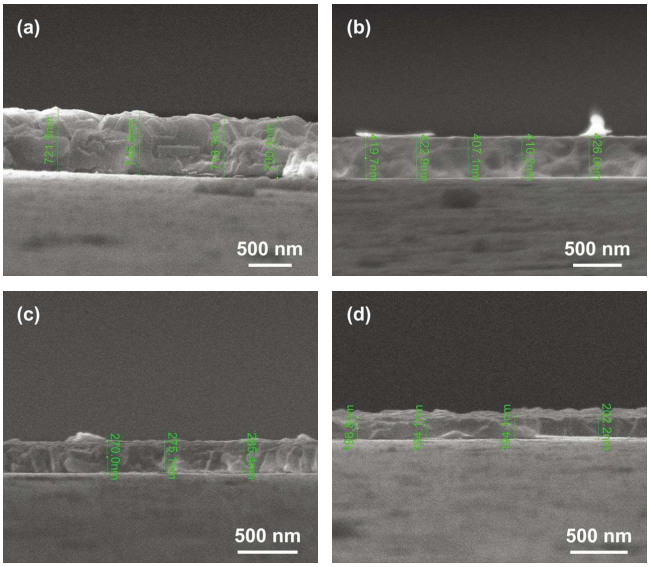


Fig. 1. SEM images of the cross section of the MgB_2 spherical shell. The cross sections were prepared by the wet-etching method. The deposition times of the shells were (a) 32 min, (b) 20 min, (c) 14 min, and (d) 12 min.

Figure 1 confirms that it is effective to fabricate thinner MgB_2 spherical shells by decreasing the deposition time during the deposition process. To see how the shell thickness reduces with reducing the deposition time, we have plotted the thickness of the shell against the deposition time, as depicted in Fig. 2. Here, the results yielded from the cross sections prepared by both the wire-cutting and wet-etching methods are summarized, and the thickness data and error bars represent, respectively, the average and errors of all the readings from all the SEM images taken for each shell. We can observe that the thicknesses determined from both methods are close to each other within their uncertainties for shells with the same deposition times. This demonstrates the consistency between the two methods and the reproducibility of the shell depositions across different samples. It is shown that, within the range of the deposition time investigated, the thickness of the MgB_2 shell exhibits roughly a linear reduction upon the decrease of the deposition time, falling from about 720 nm to 200 nm with a reduction rate of about 25 nm/min, as indicated by a linear fit to the data which is shown by a dashed line in Fig. 2. In the present work, the thinnest shell fabricated is 200 nm thick with a deposition time of 12 min. The possibility of depositing even thinner shells using even shorter deposition times remains to be explored. In particular, it would be interesting to see whether the shell thickness persists to decrease linearly upon reducing the deposition time when approaching the ultrathin regime. This could be the subject of a future study.

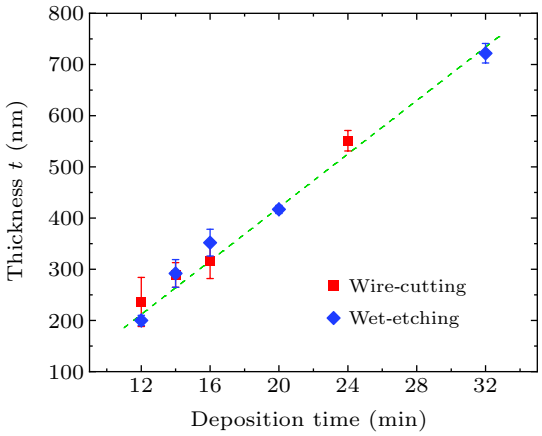


Fig. 2. Thickness of the MgB_2 shell as a function of the deposition time. Results from both the wire-cutting and wet-etching methods are plotted. The dashed line is a linear fit to the data, serving as a guide to the eye.

To examine how the surface morphology and deposition mode of the MgB_2 shell evolve as its thickness decreases, SEM images have been taken of the shells with varying thicknesses. Figure 3 compares the surface morphology of the 720 nm thick (Fig. 3(a)), 550 nm thick (Fig. 3(b)), 320 nm thick (Fig. 3(c)), and 200 nm thick (Fig. 3(d)) shells. We can see that for all shells the surface morphology exhibits a common feature in that the MgB_2 spherical film is polycrystalline, consisting of thin hexagonal grains which are oriented randomly and tightly connected. Such structure and morphology are similar to those observed in the 1 μm thick MgB_2 shell from our previous work,[18] indicating that the deposition mode of the MgB_2 shell remains largely unchanged as the thickness decreases. On the other hand, Fig. 3 also reveals that, as the shell thickness decreases, the lamellar hexagonal-shaped grains, namely, the constituent units of the film, become increasingly thinner and smaller. The thin grains of the 200 nm thick shell (Fig. 3(d)) are about half the size and thickness of the grains of the 550 nm thick shell (Fig. 3(b)). It suggests that, concomitant with the increase of the shell thickness,

the MgB_2 grains of the shell grow to get larger and thicker as we increase the deposition time.

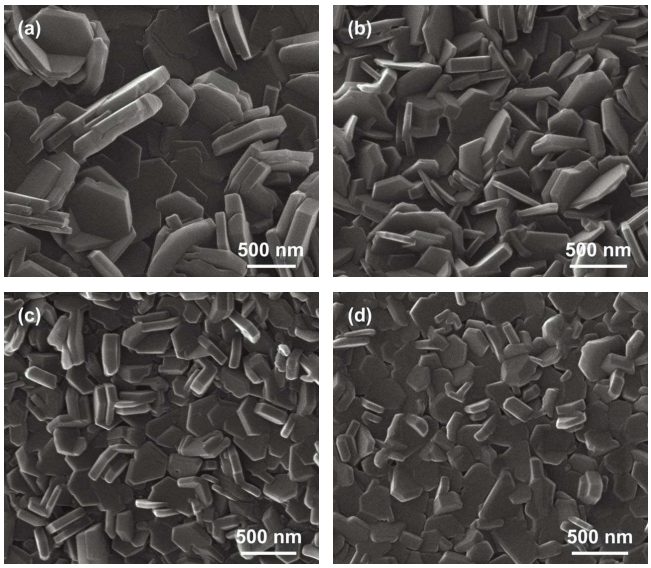


Fig. 3. SEM images of the surface morphology of the MgB_2 spherical shell. The thicknesses of the shells are (a) 720 nm, (b) 550 nm, (c) 320 nm, and (d) 200 nm, corresponding to deposition times of 32 min, 24 min, 16 min, and 12 min, respectively.

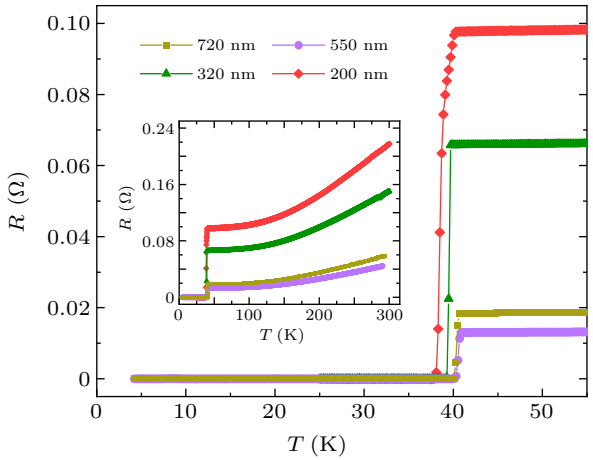


Fig. 4. Superconducting transition of the MgB_2 spherical shells with varying thicknesses, probed through the resistance measurements under zero magnetic field. The inset shows the *R*–*T* curves of the shells across the full temperature range measured.

We next explore the superconductivity of the fabricated MgB_2 shells. Figure 4 shows the superconducting transition of the shell as manifested in the electrical resistance measurement. The temperature dependence of the resistance in the full temperature range measured is plotted in the inset of Fig. 4, which shows that, at low temperatures, all shells exhibit a sharp superconducting transition at nearly the same temperature and, above the transition, the resistance–temperature (*R*–*T*) curves essentially shift upwards as the thickness of the shell decreases. The region around the superconducting transition is further enlarged in the main panel of Fig. 4, from which we can see, with decreasing the shell thickness, the superconducting transition overall moves down a little bit to lower temperatures. This could be related to the evolution of the morphology of the shell with variation of the shell thickness as unveiled in Fig. 3 and described above. The slightly inferior crystallinity of the shell with smaller and thinner MgB_2 grains, together with possibly associated evolution of the tensile strain in the shell,[24,25] might lead to the slight decline in temperature of the superconducting transition as the thickness of the shell decreases. Nonetheless, it shows that the superconducting transition temperature T_c of the shell remains high and, for the thinnest shell of 200 nm, the superconducting transition still finishes by displaying zero resistance at a temperature above 38 K, suggesting that the superconductivity has been maintained well in the MgB_2 spherical shells as we reduce the shell thickness.

The superconductivity of the MgB_2 spherical shell is further probed via the magnetization measurement, as depicted in the main panel of Fig. 5. It shows that all shells exhibit the onset of the diamagnetic transition at close temperatures of 39–40 K, corroborating the high T_c of the shells as given by the resistance measurement. With decreasing temperature, the shells complete the diamagnetic transition and enter the full superconducting diamagnetic state with a constant diamagnetic moment m which is nearly the same for all shells. As the shell becomes thinner, the temperature marking the completion of the diamagnetic transition and the onset of the full diamagnetic state becomes a bit lower, resulting in a slightly wider regime of the diamagnetic transition. In a previous study of 1 μm thick MgB_2 shells, it was found that when the lower critical field H_{c1} of the shell increases with decreasing temperature to be above the applied field of 20 Oe in the magnetization measurement, the shell finishes the diamagnetic transition and starts to enter the full diamagnetic state.[18] In light of this, it may be suggested that, as the shell becomes thinner, the H_{c1} of the shell becomes a bit lower, which then leads to the slightly wider regime of the diamagnetic transition by shifting the onset temperature to the left of the full diamagnetic state. Further measurements of the H_{c1} of the shells are desired to check this hypothesis. To quantify the full diamagnetic state, the magnetic susceptibility χ of the shells has been determined and shown by the right axis in Fig. 5. The χ has been calculated from the measured χ_{exp} with correction by considering the demagnetization factor $N = 1/3$ for a sphere,[26] that is, $\chi \simeq \chi_{exp}(1-N)$. With the applied field H and the measured moment m, the $\chi_{exp} = M_{exp}/H$ in SI units, where $M_{exp} = m/V$ is the magnetization and $V = \pi d^3/6$ is the volume of the sphere (d the diameter) which is enclosed by the circular supercurrent in the outer MgB_2 shell. Figure 5 illustrates that, in the full diamagnetic state showing a constant m after the diamagnetic transition, the χ is approximately between -1.10 and -1.08, which is quite close to -1, indicating the presence of ideal diamagnetism of the shells. The approximation used in correcting the demagnetization effect,

along with the uncertainty in the actual applied field, might contribute to the χ slightly deviating from -1. This ideal diamagnetism indicates that the shells are uniform, without voids across the entire spherical surface, which ensures the realization of the full Meissner effect in all fabricated shells as the thickness decreases from 720 nm to 200 nm. A photograph of one MgB_2 shell is shown in the inset of Fig. 5.

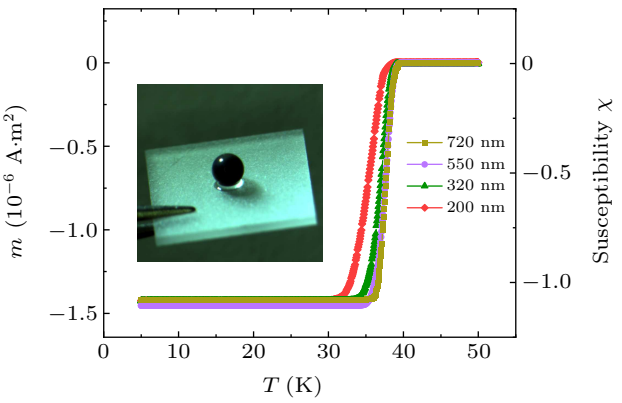


Fig. 5. Superconducting diamagnetic transition of the MgB_2 spherical shells with varying thicknesses, probed through the magnetization measurements at $H = 20$ Oe after ZFC. The right axis plots the magnetic susceptibility χ of the shell, determined from the measured magnetic moment m (left axis) by taking the demagnetization factor $N = 1/3$ for a sphere into account. The inset shows an optical image of the 200 nm thick shell sitting on a 5×5 mm^2 sapphire substrate.

Figure 6 summarizes the T_c of the shells, as determined from both the resistance and magnetization measurements. For the resistance measurement, the T_c is defined as the midpoint of the superconducting transition with error bars representing the transition width between the onset temperature T_c^{onset} and the zero-resistance temperature T_c^{zero}. For the magnetization measurement, the T_c is determined by the onset of the diamagnetic transition. It shows that the T_c values yielded from both measurements are in good agreement with each other, although, overall, the T_c from the magnetization is a bit lower than that from the resistance, as observed before in MgB_2 thicker shells[18] and bulk samples,[27] and generally in other superconducting materials,[28] which could be ascribed to the subtle differences between the two measurements in that the onset of the diamagnetic signal usually requires more regions of the sample to be superconducting for establishing macroscopic supercurrent loops to shield the applied magnetic field, as has been discussed in the literature.[18,28] By reducing the thickness, the T_c is almost the same for the shells of 720 nm and 550 nm thick, and then exhibits a slight decrease as the thickness varies from 550 nm to 200 nm. This decrease in T_c is rather mild and for the 200 nm thick shell, as aforementioned, the T_c remains above 38 K, that is, close to the value in bulk MgB_2. This retention of the high T_c close to the bulk value with reducing thickness is important for potential applications of the MgB_2 shells in areas such as ICF which requires an elevated operating temperature at around 20 K.[13] In view of previous works reporting a degradation of T_c to about 33 K or 24 K in MgB_2 spherical shells as fabricated by other methods,[16] the present result demonstrates the virtue of the HPCVD method and shows that it is experimentally achievable to fabricate MgB_2 spherical shells with reduced thickness while maintaining their good superconductivity.

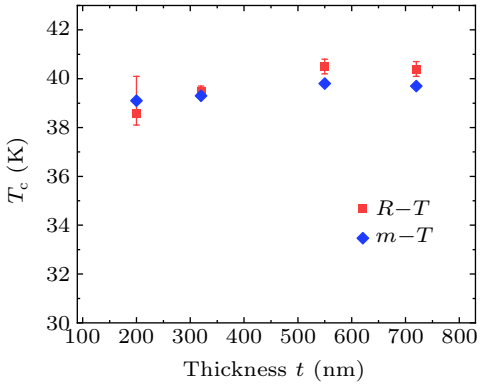


Fig. 6. Thickness dependence of the superconducting transition temperature T_c of the MgB_2 spherical shells as determined from the resistance (R–T) and magnetization (m–T) measurements.

Besides the T_c, the superconducting critical current density J_c is another important factor for the application prospect of thin MgB_2 spherical shells in areas like ICF, as it measures the superconducting current-carrying capability of the shell, thereby influencing critically the superconducting magnetic levitation properties such as the levitation force and levitation height in potential ICF applications.[8,9,17] Figure 7(a) shows the isothermal magnetization hysteresis loops measured on the thinnest MgB_2 shell of 200 nm, from which the J_c of the shell was extracted and displayed in Fig. 7(d). We observe that the magnetization hysteresis loops in Fig. 7(a) are similar to those of the 1 μm thick MgB_2 shell as reported in our previous work,[18] in terms of both the temperature evolution and field dependence, except that the m–H loops become tilted suggesting the appearance of a paramagnetic-like contribution superimposed on the superconducting irreversible magnetization. Indeed, when we measured the m–H curves at 50 K and 70 K (i.e., above the T_c of the shell), an apparent paramagnetic-like signal was observed, as depicted in Fig. 7(b), which shows that the signal exhibited negligible hysteresis and remained unchanged between the two temperatures. This signal is suspected to originate from the presence of potential magnetic impurities mixed in the sample rod, and its precise origin requires further investigation. By focusing on the superconducting irreversible magnetization, this background magnetic signal was subtracted from the m–H loops, as illustrated in Fig. 7(c), and the widths Δm of the hysteresis loops were determined as $\Delta m \equiv m^+ - m^-$, where m^+ (m^-) is the magnetic moment when decreasing (increasing) the magnetic field. The J_c of the shell was then extracted from Δm

according to the relation[18]

$$J_c = \frac{2\Delta m}{\pi g(s_0)(r+t)^4}, \tag{1}$$

which is given for a superconducting spherical shell based on the critical state model.[29] Here, r is the radius of the underlying sphere, t is the thickness of the outer superconducting shell, $s_0 = 1/(1+t/r)$, and $g(s_0)$ is a numerical factor which is closely approximated by

$$g(s_0) \doteq -1.15455 + 7.64165 s_0 - 6.4871 s_0^2,$$

when $0.98 \leq s_0 \leq 1$. With the parameters $r \simeq 500$ μm, $t \simeq 200$ nm, and $s_0 \simeq 0.9996$. The J_c of the 200 nm thick shell has been determined through Eq. (1), as plotted in Fig. 7(d) as a function of applied magnetic field with an inset showing a magnification of the low-field regime. Near zero applied field, it is observed that the J_c is above 10^6 A/cm^2 for all temperatures measured, showing a peak value of about 1.1×10^7 A/cm^2 at 15 K. At 5–12 K, the J_c is in the range 7.1×10^6–9.1×10^6 A/cm^2, lower than that at 15 K. This result arises from the smaller magnetization peaks near zero field in the m–H hysteresis loops at 5–12 K than at 15 K, as magnified in the inset of Fig. 7(a). The suppression of the loop peak at low temperatures can be attributed to the occurrence of flux jumps in the shell, as previously observed in MgB_2 thicker shells and planar films,[18,30,31] which, widely considered to be the result of a thermo-magnetic instability, would trigger an avalanche of flux motion and a suppression of J_c at low fields. Above 15 K, the J_c decreases steadily from 8.0×10^6 A/cm^2 at 20 K to 1.9×10^6 A/cm^2 at 32 K. It is noteworthy that these values of J_c are comparable to those reported for high-quality epitaxial MgB_2 thin films,[30–33] which would be beneficial for ensuring the shell's good magnetic levitation performance as required in potential applications such as ICF.[8,9,17] In moderate applied fields, Fig. 7(d) shows that the behaviour of the J_c is also encouraging. For instance, at 20 K, the J_c is 8.6×10^5 A/cm^2 at 1 T and 2.1×10^5 A/cm^2 at 2 T, comparable to that of carbon-doped or oxygen ion-irradiated MgB_2 films[34,35] which are widely recognized to have higher J_c in applied fields among the various fabricated MgB_2 thin films.[32] It suggests that, when placed in the mixed state under moderate magnetic fields, the fabricated MgB_2 shell with reduced thickness also holds promise for potential superconducting levitation applications. Finally, it is noted that the J_c depicted in Fig. 7(d) is overall higher than that of the 1 μm thick MgB_2 shell as reported in our previous work.[18] This difference might be attributed to the smaller grain size in the 200 nm thick shell,[32,34] which warrants further explorations.

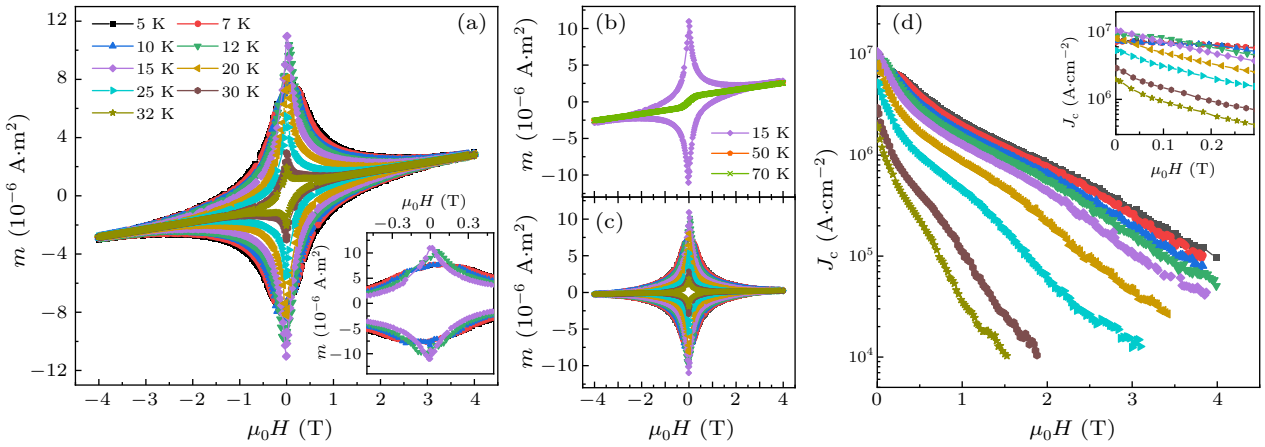


Fig. 7. (a) Isothermal magnetization hysteresis loops of the 200 nm thick MgB_2 spherical shell. The inset magnifies the m–H loops in the low-field region at 5–15 K, showing a suppression of the loop peak near zero field below 15 K. (b) The m–H curves at 50 K and 70 K, i.e., above the T_c of the shell, plotted together with the hysteresis loop at 15 K. (c) The m–H hysteresis loops in (a) after subtracting the background signal at 50 K shown in (b). (d) The superconducting critical current density J_c determined from (c) as a function of applied magnetic field with the inset zooming in on the low-field regime.

4. Summary

In summary, we have succeeded in fabricating MgB_2 spherical shells with reduced thickness by HPCVD. By tuning the deposition time, a set of MgB_2 shells with thickness varying from 720 nm to 200 nm has been grown on 1 mm diameter Si_3N_4 spheres. The spherical shells feature a polycrystalline structure characterized by randomly oriented, well-connected hexagonal grains, along with a shrinkage in both size and thickness of the grains as the thickness of the shell decreases. Notably, all shells exhibit a T_c of 38–40 K, that is, close to the value in bulk MgB_2, and ideal diamagnetism at low temperatures, indicating that the high-T_c superconductivity of MgB_2 has been well preserved in the spherical shells as the thickness is reduced. It is further encouraging to find that the thinnest shell of 200 nm has a J_c of 8.0×10^6 A/cm^2 and 2.1×10^5 A/cm^2 at 20 K in zero and 2 T applied field, respectively, which suggests that the shell has an excellent supercurrent-carrying capability not only in zero field but also in moderate magnetic fields. Collectively, this demonstrates

the feasibility of fabricating MgB_2 spherical shells that possess high T_c and high J_c, while being thin enough to be considered acceptable for potential magnetic levitation applications in ICF. Further investigations on additional superconducting properties of the spherical shells, such as their superconducting critical fields, are desired, which would provide valuable information for evaluating the magnetic levitation properties of the shell. It would also be intriguing to explore the fabrication of even thinner MgB_2 shells. We observe that the thickness of 200 nm is already comparable to the magnetic penetration depth of MgB_2 at zero temperature, which is reported to range from approximately 40 nm to 300 nm depending on the cleanliness of the sample.[36,37] Therefore, the fabrication of MgB_2 spherical shells with a thickness lower than 200 nm may not only have implications for potential ICF applications, but also offer the possibility to study the interplay among the three-dimensional spherical geometry,[38] the mesoscopic scale, and the multiband effect of MgB_2,[32,39] which might give rise to novel emergent physical phenomena.

Acknowledgment

We thank Li X J (China Academy of Engineering Physics) for helpful discussions.

References

[1] Buchman S, Lipa J A, Keiser G M, Muhlfelder B and Turneaure J P 2015 *Class. Quantum Grav.* **32** 224004
[2] Goodkind J M 1999 *Rev. Sci. Instrum.* **70** 4131
[3] Everitt C W F, DeBra D B, Parkinson B W, *et al.* 2011 *Phys. Rev. Lett.* **106** 221101
[4] Everitt C W F, Muhlfelder B, DeBra D B, *et al.* 2015 *Class. Quantum Grav.* **32** 224001
[5] Huang X, Hu X, Cui C, Wang H, Niu F, Zhang Y, Wang L, Wang Q, Hao X, Liu M, Chen X and Yang Y 2022 *IEEE Trans. Instrum. Meas.* **71** 9502410
[6] Merlet S, Le Moigne N, Métivier G P, Bernard J D, Little F, Boy J P, Rosat S, Gabalda G, Seoane L, Bonvalot S, Champollion C, Mémin A, Maia M and Charade O 2024 *IEEE Instrum. Meas. Mag.* **27** 24
[7] Nagamatsu J, Nakagawa N, Muranaka T, Zenitani Y and Akimitsu J 2001 *Nature* **410** 63
[8] Li X, Xiao T, Chen F, Zhang Y, Li X and Wu W 2018 *Matter Radiat. Extremes* **3** 104
[9] Smalyuk V A, Robey H F, Alday C L, *et al.* 2018 *Phys. Plasmas* **25** 072705
[10] Tollefson J and Gibney E 2022 *Nature* **612** 597
[11] Tollefson J 2024 *Nature* **625** 11
[12] Weber C R, Casey D T, Clark D S, *et al.* 2017 *Phys. Plasmas* **24** 056302
[13] Gibson C R, Atkinson D P, Baltz J A, Brugman V P, Coffield F E, Edwards O D, Haid B J, Locke S F, Malsbury T N, Shiromizu S J and Skulina K M 2009 *Fusion Sci. Technol.* **55** 233
[14] Haan S W, Lindl J D, Callahan D A, *et al.* 2011 *Phys. Plasmas* **18** 051001
[15] Betti R and Hurricane O A 2016 *Nat. Phys.* **12** 435
[16] Bayu Aji L B, Baker A A, Bae J H, Beckham J L, Jacob R E, Shin S J, McCall S K and Kucheyev S O 2020 *Thin Solid Films* **710** 138260
[17] Li X, Wang H, Li Z, Zeng Y, Zhong M and Wang Y 2022 *J. Supercond. Nov. Magn.* **35** 3537
[18] Xu T Q, Sun R N, Zhao J X, Wang Y, Wang F R and Gan Z Z 2023 *Supercond. Sci. Technol.* **36** 095006
[19] Regan S P, Epstein R, Hammel B A, *et al.* 2013 *Phys. Rev. Lett.* **111** 045001
[20] Gu J, Dai Z, Zou S, Ye W, Zheng W, Gu P and Zhu S 2017 *Matter Radiat. Extremes* **2** 9
[21] Kritcher A L, Clark D, Haan S, Yi S A, Zylstra A B, Callahan D A, Hinkel D E, Berzak Hopkins L F, Hurricane O A, Landen O L, MacLaren S A, Meezan N B, Patel P K, Ralph J, Thomas C A, Town R and Edwards M J 2018 *Phys. Plasmas* **25** 056309
[22] Zhang C, Wang Y, Wang D, Zhang Y, Liu Z H, Feng Q R and Gan Z Z 2013 *J. Appl. Phys.* **114** 023903
[23] Cheng S H, Zhang Y, Wang H Z, Li Y L, Yang C and Wang Y 2018 *AIP Adv.* **8** 075015
[24] Hur N, Sharma P A, Guha S, Cieplak M Z, Werder D J, Horibe Y, Chen C H and Cheong S W 2001 *Appl. Phys. Lett.* **79** 4180
[25] Pogrebnyakov A V, Redwing J M, Raghavan S, Vaithyanathan V, Schlom D G, Xu S Y, Li Q, Tenne D A, Soukiassian A, Xi X X, Johannes M D, Kasinathan D, Pickett W E, Wu J S and Spence J C H 2004 *Phys. Rev. Lett.* **93** 147006
[26] Tinkham M 2004 *Introduction to Superconductivity* 2nd edn. (New York: Dover)
[27] Lee S, Mori H, Masui T, Eltsev Y, Yamamoto A and Tajima S 2001 *J. Phys. Soc. Japan* **70** 2255
[28] Poole C P Jr, Farach H A, Creswick R J and Prozorov R 2007 *Superconductivity* 2nd edn. (London: Academic)
[29] Bhagwat K V and Chaddah P 1990 *Physica C* **166** 1
[30] Zhao Z W, Li S L, Ni Y M, Yang H P, Liu Z Y, Wen H H, Kang W N, Kim H J, Choi E M and Lee S I 2002 *Phys. Rev. B* **65** 064512
[31] Liu L, Lee J M, Han Y, Song J, Kim C, Suk J, Kang W N, Liu J, Jung S and Park T 2023 *Chin. Phys. B* **32** 127402
[32] Xi X X 2009 *Supercond. Sci. Technol.* **22** 043001
[33] Wang H Z, Li Y L, Wang Y and Gan Z Z 2020 *Physica C* **569** 1353587
[34] Zhuang C G, Meng S, Yang H, Jia Y, Wen H H, Xi X X, Feng Q R and Gan Z Z 2008 *Supercond. Sci. Technol.* **21** 082002
[35] Wang J, Zhuang C G, Li J, Wu Z W, Li S, Chu H F, Feng Q R and Zheng D N 2009 *Supercond. Sci. Technol.* **22** 045020
[36] Golubov A A, Brinkman A, Dolgov O V, Kortus J and Jepsen O 2002 *Phys. Rev. B* **66** 054524
[37] Jin B B, Dahm T, Iniotakis C, Gubin A I, Choi E M, Kim H J, Lee S I, Kang W N, Wang S F, Zhou Y L, Pogrebnyakov A V, Redwing J M, Xi X X and Klein N 2005 *Supercond. Sci. Technol.* **18** L1
[38] Fomin V M and Dobrovolskiy O V 2022 *Appl. Phys. Lett.* **120** 090501
[39] Yang H, Liu Y, Zhuang C, Shi J, Yao Y, Massidda S, Monni M, Jia Y, Xi X, Li Q, Liu Z K, Feng Q and Wen H H 2008 *Phys. Rev. Lett.* **101** 067001